Proceedings of PSFVIP-5
5th Pacific Symposium on Flow Visualisation and Image Processing
27-29th September 2005, Australia

PSFVIP-5-244

CFD MODELLING OF SYNTHETIC JETS IN A BOUNDARY LAYER AT ADVERSE PRESSURE GRADIENT

Tetsuya Ozawa[1], Guang Hong[2], A. N. F. Mack
Faculty of Engineering, University of Technology Sydney,
PO Box123, Broadway, NSW 2007, Australia

Abstract: The flow field experimentally realized by the wind tunnel for the investigation of the control of boundary layer separation by synthetic jets is numerically modelled. Results of the simulations show good agreement with facts in experiment and some features of the flow control are discussed.

1 Introduction

A synthetic jet actuator (SJA) is a jet generator which requires zero mass input, yet can produce non-zero momentum output. A unique feature of synthetic jets is that they can be formed entirely from the working fluid of the flow system in which they are deployed and can transfer linear momentum to the flow system without net mass injection across the flow boundary. Moreover, synthetic jets can be produced over a broad range of length and timescale. These unique features of synthetic jet actuator make them attractive fluidic actuators for various types of flow control applications. The potential for controlling flow has been shown in previous research, such as the controlling of transition [1], delaying of separation [2], effecting vortex control [3], enhancing mixing [4] and maximizing the lift by minimizing the separation on the suction side of an airfoil [5].

As shown in the schematic in Figure 1, a synthetic jet actuator consists of a cavity and oscillating material, and the jet is synthesized by oscillatory flow, blowing and suctioning through a small orifice. The flow is induced by a vibrating membrane which is the bottom walls forming the cavity. In our previous experimental study conducted by Hong [6], piezoelectric material was applied for driving the oscillating diaphragm, as it promotes desirable characteristics, such as low power consumption, fast response, reliability, and low cost [7].

Computational fluid dynamics (CFD) has been used integrally with experiments in developing synthetic jet actuators for active flow control. Although there are still many 'unknowns' in modeling the fluids, the challenge of CFD is now compounded with the introduction of active flow control technologies [8]. Extensive work has been conducted on numerical modeling of the synthetic jet actuator itself for simulating the synthetic jets

---

[1] Exchange student at UTS, currently Master's degree student at the Tokyo Institute of Technology, Japan.
[2] Author for correspondence, Fax +61 2 9512 2655, Email: guang.hong@uts.edu.au

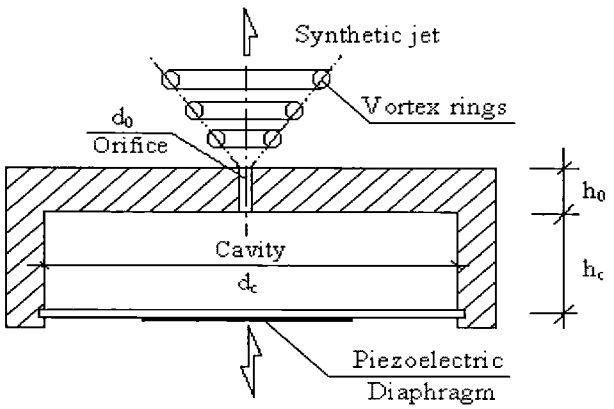

Figure 1: Schematic of the synthetic jet actuator, where d_0 is the orifice diameter, d_c is the diameter of the membrane, h_0 is the depth of the orifice and h_c is the maximum height of the cavity [6]

generated in a quiescent external flow condition (without fluid flow crossing the jet) [9,10,11,12]. In this numerical modeling, the neighbourhood of the jet exit was simulated. Kral *et al* [9] aimed to model the boundary condition at the exit of the orifice of the actuator. They did not model the air flow inside the cavity but examined three different velocity distributions along the orifice. They investigated various jets, laminar and turbulent, pulsed and steady, and achieved very good agreement with experimental measurement. The models in [10,11,12] included the flow behavior in the cavity of the actuator and simulated not only the jets generated but also the compression/discharging and expansion/intake processes in the cavity. Mittal *et al* also simulated the jet at the exit of the orifice with cross flow in a boundary layer under a zero pressure gradient [11].

Prior to numerically modeling the synthetic jets interacting with the base flow to be controlled, it is necessary to have numerical model ready for the separation bubble caused by adverse pressure gradient in the boundary layer. The difficulties in modeling the separation bubble, especially the transition, have been well known. As commented by Gad-el-hak, current inaccuracies in turbulence modeling can severely degrade CFD predictions once separation has occurred [13]. The over-prediction of the production of turbulence kinetic energy and dissipation were reported in [14,15]. However, at the meantime when he pointed out the problems, Gad-de-hak also justified that the essence of separation control was the calculation of attached flows, estimation of separation location, and indeed whether or not separation would occur [13]. This has given us the confidence in using CFD as an alternative tool for developing the synthetic jet actuator and also raised our cautiousness for using CFD properly.

In comparison with the numerical simulation of synthetic jets in a quiescent condition, much less publications have reported numerical simulation of the interaction between the jets and the base flow to be controlled. This may be due to the difficulties reviewed above. Allan *et al* [16] investigated the numerical simulation of a 2-D airfoil controlled by jet. They demonstrated the CFD model coupled with the model for rigid body motion. Parekh *et al* [17] numerically simulated the experimental separation control on a thick airfoil using synthetic jet action conducted by Glezer's team [18]. Their model successfully predicted the reattachment dynamics and the dependence of controlling reattachment on forcing frequency.

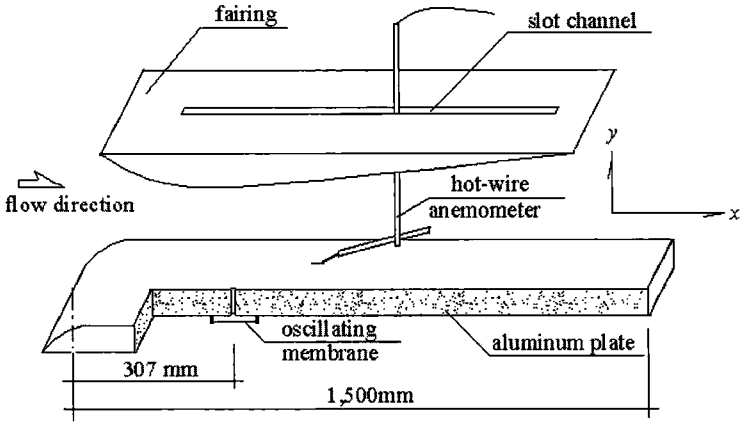

Figure 2: Experimental setting in the wind tunnel [6]

Different fluid models and numerical approaches have been consistent in development and enhancement through their applications. The turbulence models and solvers used in simulating the synthetic jets in quiescent condition include a two-dimensional incompressible flow model with Reynolds-averaged Navier-Stokes (RANS) [9] or Direct Numerical Simulation (DNS) [11], and three-dimensional model with DNS [19]. In 2-D simulation of separation control over an airfoil using synthetic jets, unsteady RANS [16] and hybrid RAND/LES derived from combining the best features of RANS and LES [17]. DNS have been used in simulating the separation bubble [20].

As reviewed above, although computations for the synthetic jet in the absence of a cross flow or for a boundary layer separation have been performed respectively, an integrated numerical model, such as that including synthetic jets in a separated boundary layer, is still being developed. Therefore, the purpose of the work reported in this paper was to develop a CFD model for numerically predicting the control effectiveness of synthetic jets on separation control, focusing particularly on the effects of synthetic jets with lower forcing frequency which is in the range of Tollmien-Schlichting (T-S) instability.

2 Numerical Methodologies

2.1 Geometry of the numerical model

2.1.1 Experimental setup and computational domain: Experiments on the synthetic jets with a cross flow were performed in an open circuit wind tunnel in the Aerodynamics Laboratory at the University of Technology, Sydney [6]. Figure 2 shows the schematic of the experimental setting in the working section. Air enters the operational section via a bell mouth inlet and a honeycomb screen section through which minimum turbulence achievable is 0.3%. A polished aluminium plate, 1500 mm × 608 mm × 25 mm, was mounted horizontally in the test section. The actuator was attached to the wall beneath the surface over which the boundary layer was formed. The orifice of the synthetic jet actuator was located on the streamwise centreline at X = 307 mm from the leading edge of the flat plate. A fairing was located above the flat plate with its angle adjustable for establishing the desired pressure gradient. The leading edge of the upper surface is of elliptical arc form and is located 1200

mm from the working section entrance. Every 25 mm along the streamwise centreline of the flat plate, static pressure taps were set and a multi-tube manometer was used to measure the pressure distribution. The instantaneous velocity in the boundary layer in the tunnel was measured by the hot-wire anemometer with a sample rate of 6 kHz.

In this study the flow field in the test section was numerically simulated, from the position 20 mm upstream of the orifice of the synthetic jets, to the end of the test section. The schematic diagram of the numerical model is shown in Figure 3. In accordance with the experimental conditions, the flow field in numerical simulation is scaled. x corresponds to the streamwise direction, y the wall-normal direction and z the spanwise direction in the coordinate system. The dimensions of the computational domain are L_x = 200mm, L_y = 60mm and L_z = 45 mm in streamwise, wall-normal and spanwise directions respectively. The method for determining the domain is discussed in the following section. For comparison with the experimental results, X and x are employed as coordinate variables representing the position in x-direction, where $x = 0$ and $X = 307$ correspond to the location of the centreline of the orifice and $X = 0$ at the leading edge of the flat plate.

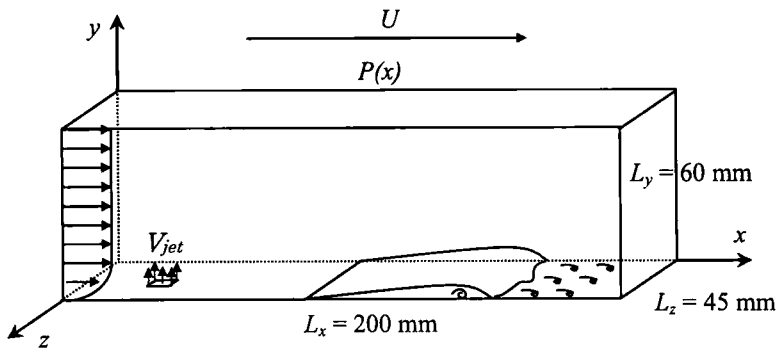

Figure 3: Computational domain of synthetic jets and a boundary layer

2.1.2 Boundary conditions: The non-slip boundary condition was set along the bottom of the computational domain. The orifice of the synthetic jets is placed at the centre in spanwise direction, $z = 0$. The flow along the edge of the domain in spanwise direction is assumed to be symmetric. Applicable to both boundaries, the symmetric boundary conditions generate a flow of period length $2 \times L_z$.

Since the velocity profiles along inlet boundary at X = 287 mm was not measured in the experiment, the modelling of the inflow is required. In order to obtain a realistic flow field, appropriate velocity profiles of a laminar boundary layer, along with free stream and disturbance velocity in a boundary layer (along the inlet boundary), should be predetermined in the numerical simulation. Blasius velocity profile of a laminar boundary layer is used for the inlet boundary condition near the plate, at which point the boundary layer thickness was adjusted using the experimental results. Based on the fact that the flow travels upward as well as downstream, wall-normal velocity component in the free stream linear to the distance from

the flat plate is introduced. The amplitude of the velocity in wall-normal direction at the top of the domain was adjusted according to previous simulations and the velocity in downstream direction was determined to maintain constant velocity amplitude. Artificial-minute disturbance in wall-normal direction at the inlet is given by generated Gaussian random number. The amplitude of the disturbance is selected as 1%, 2% and 3% of the free stream velocity. This minute disturbance is to induce the development of the turbulence structure on the separation of a boundary layer. The spanwise component is set as zero at this boundary.

In many of previous numerical studies of a boundary layer separation, the boundary condition at the upper surface of computational domain is given by means of fixing the velocity, which is a suction-blowing distribution of $V_{top}(x)$ [21, 22], thus fixing the separation and the reattachment points, as otherwise the entire wind tunnel is included in the model [23]. In this simulation, the position of the separation and the reattachment of a boundary layer vary with the synthetic jet's effect. Therefore, given the value of the velocity along the top surface of the domain, this methodology proves unsuitable. Instead of velocity profile, the pressure profile is employed with the following outlet boundary condition.

$$P(x, L_y, z, t) = P_{top}(x) \tag{1}$$

It is noted here that since the domain in wall-normal direction was empirically set high enough for velocity field at the top not to be influenced by the short bubble of a boundary layer, it is possible to simulate the steady free stream velocity profile under adverse pressure gradient regardless of the boundary layer motion close to the flat plate. The setting of the models' height in this simulation was sufficiently examined and carefully decided upon. In doing so, the free stream velocity and pressure profile, invoking the separation of a boundary layer, observed in the wind tunnel was realized, where the free stream travels in a north-easterly direction. Here, the pressure distribution on the flat plate obtained in the experiment, including its drop by the separation bubble, was slightly modified to estimated profile for the steady free stream and employed for the boundary condition along the top surface.

2.2 Large Eddy Simulation

The governing equations for this flow are the equation of continuity and incompressible three-dimensional Navier-Stokes equations, (2) and (3) respectively.

$$\frac{\partial u_i}{\partial x_i} = 0 \tag{2}$$

$$\frac{\partial u_i}{\partial t} + u_j \frac{\partial u_i}{\partial x_j} = -\frac{1}{\rho}\frac{\partial P}{\partial x_i} + \nu \frac{\partial^2 u_i}{\partial x_j \partial x_j} \tag{3}$$

where, u_i is the velocity in each direction, x_i is the space coordinate, P is the absolute pressure, ν is the kinematic viscosity and ρ is the fluid density. Large Eddy simulation (LES) was employed to compromise the computational resources and the accuracy of the numerical simulation. By filtering Equation (2) and Equation (3) in space, grid-filtered governing equation and Sub-grid scale stress (SGS) terms were produced. Dynamic Smagorinsky model was used for the approximation of SGS stress terms as previous numerical researches have proven the reliability of this model. Filtered Equation (2) and Equation (3) were discretised in space using a second-order central difference scheme with the second-order Crank-Nicolson method employed for time integration. For the numerical stability of the calculation, the

convection term is integrated by means of a hybrid method of first-order upwind difference scheme and second-order central difference scheme. $240\times60\times40$ grid points were used consisting of the concentrated mesh very near the wall and the orifice of the synthetic jet actuator using trigonometric function. CFD-ACE was used as a solver of governing equations. Reynolds number Re_δ, based on the boundary layer thickness at the inlet and the free stream velocity, was 500.

2.3 Modelling of the synthetic jets

The synthetic jet actuator used in the experiments consisted of a membrane located at the bottom of a small cavity and orifices in the plane opposite the membrane. As illustrated in Figure 1, the diameter of the orifice, d_0, was 0.5 mm and the membrane of this actuator, driven by a sine wave from a standard electrical signal generator, was a thin circular brass disc, 0.25 mm in thickness, placed firmly at its perimeter. In the numerical study, the physical cycle in the actuator was not numerically simulated. Based on experimental measurement of the jet velocity at the centreline of the jet at the exit of the orifice, the boundary condition at the orifice's exit was defined by the velocity which was a sine wave function, as follows.

$$V = V_{jet}\sin(2\pi ft) \tag{4}$$

where, f is the forcing frequency, t is time and V_{jet} is the maximum jet velocity in the direction of the centreline of jet at the exit of the orifice. The phase of this sine wave function was assumed to be zero, and the restricting effect of the orifice on flow was not considered. The turbulent level was included in (4). For ease in mesh construction, the shape of orifice was assumed as square. The input velocity, V_{jet}, and the forcing frequency, f, were determined according to the experimental results [6].

3 Results and Discussion

3.1 Verification of the numerical model

3.1.1 Velocity profile: Figure 4 shows the comparison of the mean and fluctuating velocity profiles in the separation region obtained from the experiment and the numerical simulation. The mean velocity is normalized by the free stream velocity measured at x = -20 mm, 8 m/sec. The fluctuating velocity is normalized by the estimated maximum fluctuating velocity in the turbulence, 1.5 m/sec. The inflection points in the mean velocity profiles at the y positions close to the wall can be noticed in the region of x = 60~120 mm. In this region the fluctuating velocity is relatively low. Both mean and fluctuating velocity profiles indicate that the boundary layer separation is laminar. At a position between x = 140 and x = 160 mm, the boundary layer reattaches to the wall and the mean velocity profile at x = 160 mm represents the acute velocity gradient close to the wall, which is characterized by a turbulent boundary layer. As also shown in Figure 4, the development of the fluctuating velocity occurs in the separated layer, suggesting the transition from laminar to turbulent flow in a shear free flow. The fluctuating velocity of the numerical simulation shows approximately as twice as those measured in the experiment excluding that at x = 160 mm. The similarity of the shape of the profile and their competitive quantity positively supports the validity of the numerical model. Both numerical and experimental results show that at x = 160 mm, downstream of the reattachment, the breakdown of a boundary layer into the complex turbulence structure [20] occurs and a turbulent boundary layer develops. The LES sufficiently captured longitudinal vortices formed by the second instability, which induces the transition and the reattachment.

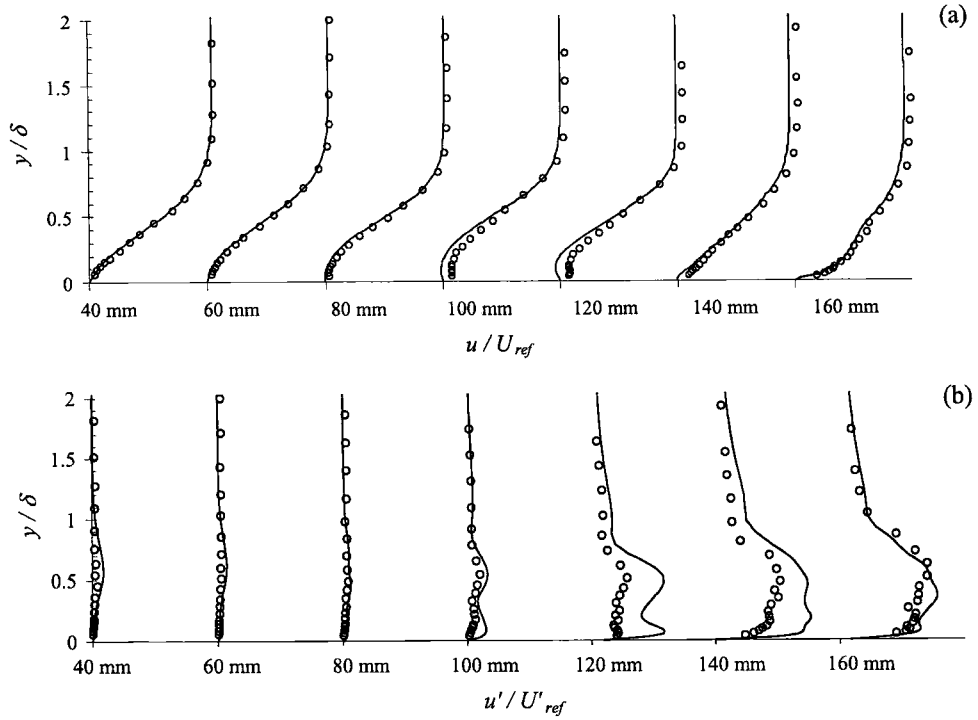

Figure 4: Velocity profiles in the separation region along the streamwise direction
(a): Mean velocity, (b): Fluctuating velocity,
Solid line: Numerical simulation, Symbol: Experiment

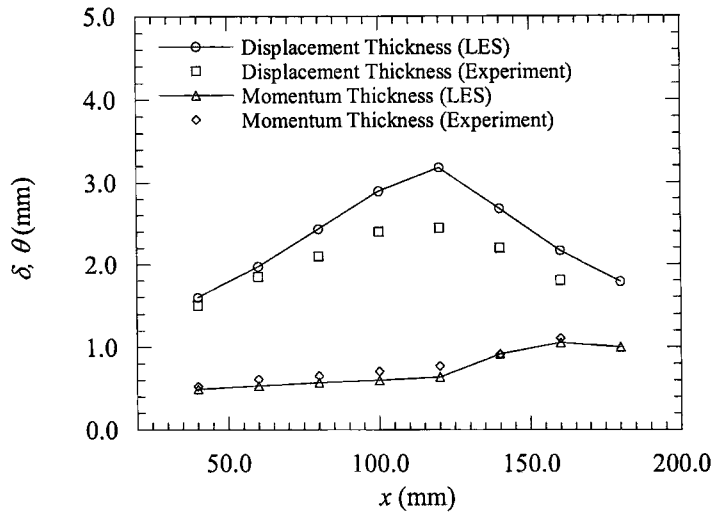

Figure 5: Variation of displacement thickness δ and momentum thickness θ in downstream direction

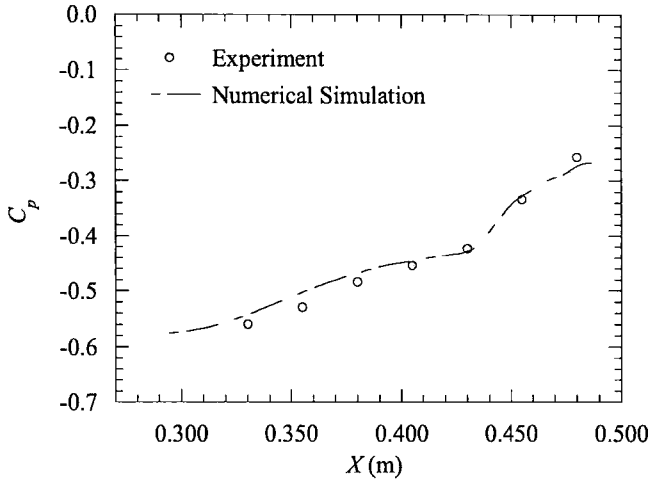

Figure 6: Pressure profile on the flat plate along the streamwise direction

3.1.2 Laminar separation bubble: Figure 5 shows the compared experimental and numerical results of the displacement boundary layer thickness and momentum boundary layer thickness in streamwise direction. As shown in Figure 5, the maximum displacement consistently occurs at a position between x = 100~120 mm in both experimental and numerical results. The variation of the displacement thickness is also consistent except that the numerical displacement thickness is greater than the experimental one. According to Hatman and Wang [24], there are distinguishing three separated-flow transition modes, transitional separation, laminar separation-short bubble and laminar separation-long bubble. The first mode of separation involves the transition from laminar flow to turbulence starting upstream of the separation point. In the latter two modes, the transition occurs downstream of the separation point by inflexible instability. The maximum displacement of the shear layer occurs at the onset of the transition and the first reattachment point has the maximum turbulence level. Therefore, the separation simulated is identified as laminar separation.

Figure 6 shows the comparison of the experimental and numerical pressure distributions in the streamwise direction. As agreed in both experimental measurement and numerical simulation, the pressure curve starts to become 'flat' around X = 380 mm (x = 73 mm) until the pressure gradient is recovered around X = 450 mm (x = 143 mm). This zone with 'flatter' pressure distribution is identified as the separation bubble. Gaster [25] proposed the two-parameter bubble criterion by means of a relationship between the momentum Reynolds number at separation, Re_θ which was denoted by the momentum thickness, θ, and the variation of the free stream velocity over the separation zone. This relation can be described by the pressure parameter, $\overline{P}$, as follows.

$$\overline{P} = \frac{\theta^2}{\nu}\frac{\Delta U}{\Delta x} \tag{5}$$

where, ΔU is the variation of the free stream velocity over the bubble, and Δx is the bubble length. Based on the momentum thickness as shown in Figure 5 and the velocity drop in the separation region numerically and experimentally obtained, the corresponding Re_θ and

$\overline{P}$ are 300 and -0.14 respectively. In accordance with this criterion, the separation can be identified as short-bubble separation, supporting the assumption for the determination of the domain in wall-normal direction given the short bubble has no influence on the free stream.

In order to investigate the influence of the disturbance level at the inlet of the computational domain on the simulation of the separation bubble, three different levels of the inlet disturbance were applied and the results are summarized in Table 1. X_A, X_B and L_S are the separation point, reattachment point and the length of the separation bubble respectively. The three levels of the disturbance in a random phase were 1%, 2% and 3% of the free stream velocity. As shown in Table 1, the length of the separation bubble decreases with the increase of the disturbance level, and the separation bubble moves upstream when the disturbance level increases. This decrease of the separation bubble length was observed in previous experimental research with various amplitudes of the disturbance [26].

Table 1: Dependency of the boundary layer separation on the disturbance level at the inlet

Disturbance (%)	X_A (mm)	X_B (mm)	L_S (mm)
1	94.0	161.0	67.0
2	88.0	151.0	63.0
3	85.0	141.0	56.0

3.2 Effect of the synthetic jets on a boundary layer separation

3.2.1: Frequency dependency: The experimental results in [6] demonstrated that the synthetic jets were effective on protecting the boundary layer flow from separation when the forcing frequency was 100 Hz which was in the frequency range of T-S instability. In order to investigate the impact of forcing frequency on control effectiveness, the numerical model preliminarily verified for simulating the separation bubble caused by adverse pressure gradient was used to simulate the synthetic jet interacting with the base flow with different forcing frequencies. The jet velocity, V_{jet} in equation (4), was 1.5 m/sec based on the experimental measurement, which was in the condition when the synthetic jet actuator was driven with a forcing amplitude of ±7.5 V. Figure 7 shows the sample result of comparing the velocity profiles at x = 120 mm along the centreline of the streamline when two forcing frequencies, 100 Hz and 800 Hz, were applied. 800 Hz is outside of the frequency range of T-S instability. As shown in Figure 7, at 120 mm downstream of the synthetic jet actuator, the mean velocity profile has a reflectional point which indicates the existence of a separation bubble in the base flow. When the synthetic jet actuator is switched on at forcing frequency of 100 Hz, the mean velocity profile is significantly changed to be 'fuller', which shows the separation disappears and that the boundary layer is turbulent. However, the synthetic jet does not show any effectiveness when it is driven at a forcing frequency of 800 Hz. The synthetic jet's behaviour predicted by this numerical model is consistent with that observed in the experiments, therefore this shows that the simplified orifice geometry is valid.

The principle of this synthetic jet is accelerating the turbulence which resists the laminar separation. The evolution of the fluctuating velocity in streamwise direction is shown in Figure 8. It can be noticed that the fluctuation with the jet off increases exponentially in the

separation zone and reaches an approximate maximum point. The cause of this rapid increase can be explained as that the disturbance at the inlet is amplified by the Kelvin-Helmortz (K-H) instability in the free shear layer flow. In the other case, when the synthetic jet of 100 Hz is switched on, the fluctuating velocity starts to increase moderately before x = 40 mm or before the separation point in the base flow, and reaches its maximum earlier than that in the base flow. This difference shows the effectiveness of the synthetic jets enhanced by the T-S instability. Comparison of the fluctuating velocity profiles with and without the jet in Figure 9 shows this effectiveness enhancement at x = 120 mm.

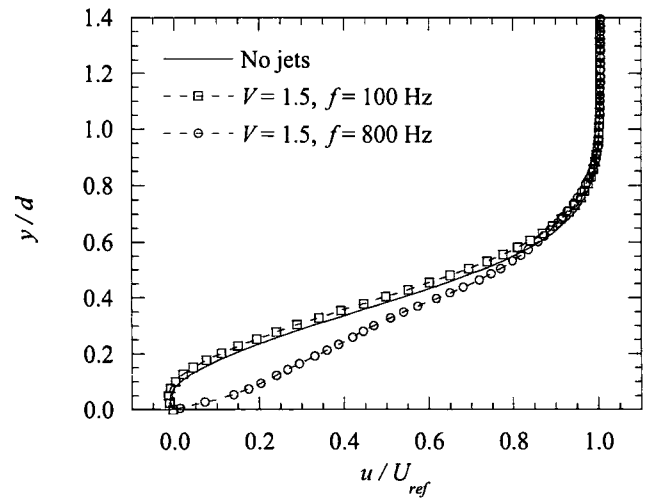

Figure 7: Mean velocity profiles on the centreline of the orifice at x = 120 mm with the synthetic jets on/off

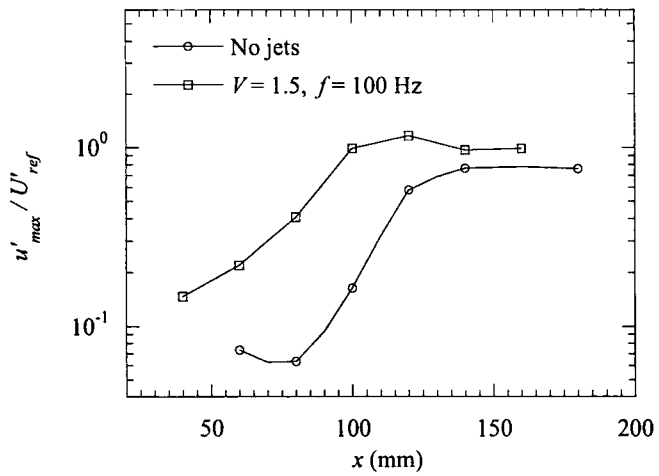

Figure 8: Development of the fluctuating velocity in the separation region along the streamwise direction with the synthetic jets on/off

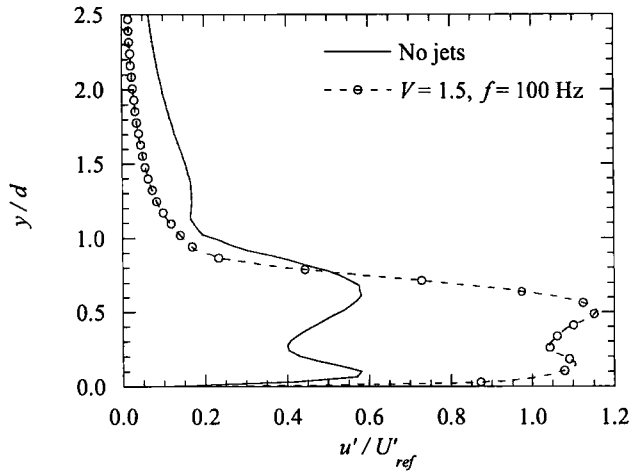

Figure 9: Fluctuating velocity profiles at x = 120 mm with the synthetic jets on/off

3.2.2: Three-dimensional view: Figure 10 shows the isosurface of the vorticity near the wall with the jet of 100 Hz on/off. It can be observed from Figure 10(a) that the isosurface of the vorticity, vortex layer, separates from the wall. The large-scale waves transfer in streamwise direction and the laminar layer breaks down into streak structure inclining in downstream direction as described in [22]. After the reattachment, the structure becomes finer and more complicated. All these demonstrate that LES is sufficiently capable to model the transition in a laminar separation boundary layer and the development of a turbulent boundary layer with limited grid points. In comparison, in Figure 10(b), the 'breaking down' occurs earlier (more upstream), spreading gradually and symmetrically in spanwise direction. The longitudinal vortex structure observed under the vortex layer seems to play an important role in accelerating the turbulence to resist the laminar separation.

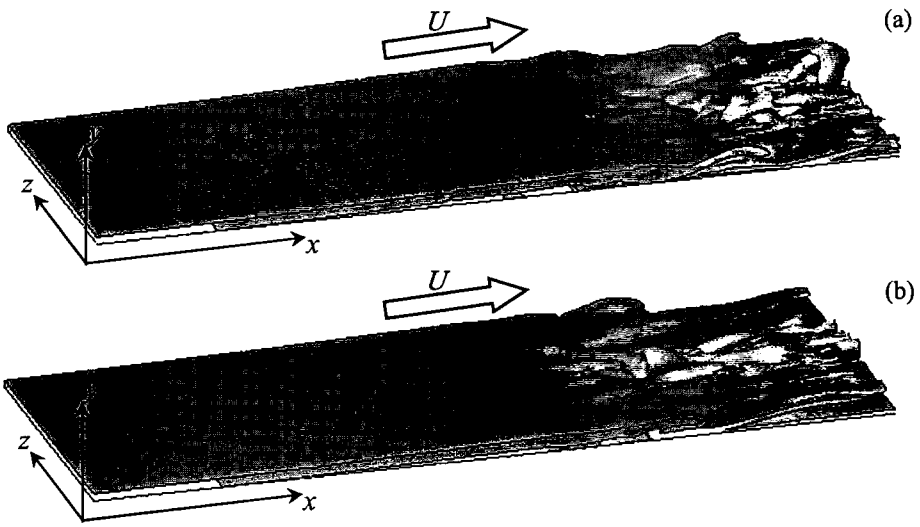

Figure 10: Isosurface of the vorticity near the wall, (a): No jets, (b): With jets of 100 Hz

4 Conclusions

Large Eddy Simulation of synthetic jets in a boundary layer under an adverse pressure gradient was carried out using Dynamic Smagorinsky model. The adverse pressure gradient causing the boundary layer separation was imposed to the boundary layer flow over a flat plate by defining the absolute values of pressure on the top of the computational domain. A separation bubble with a length of approximately 60 mm and a reattachment with a breakdown of laminar layer into complicated three-dimension structure were numerically simulated. The separation bubble in both the numerical simulation and the experiment is classified as laminar separation-short bubble according to the method of Hatman and Wang [24] and Gaster's two parameter-bursting criterions [25]. Consistent with the experimental results, the numerical simulation predicted the great effectiveness of a synthetic jet on resisting laminar separation by accelerating the turbulence, when the forcing frequency was in the range of T-S instability. This numerical study provided structural analysis of the interaction between the synthetic jets and the separation flow. It can be concluded that numerical simulation with low computational resources and satisfactory accuracy was achieved for this particular boundary layer flow. Further numerical studies of the effects of the synthetic jets with various parameters, significant for high-efficiency technology of aerodynamic devices such as lifting bodies, is to be undertaken through the implementation of a similar model in future research.

5 References

1. H.U. Meier and M. –D. Zhou, The development of acoustic generators and their application as a boundary layer transition control device, *Experiments in Fluids*, Vol.11, 93-104, 1991.
2. S.K Sinha and D. Pal, On the differences between the effect of acoustic perturbation and unsteady bleed in controlling flow separation over a circular cylinder, SAE Technical Paper, 932573, 1993.
3. F.W. Roos, Synthetic-jet microblowing for vortex asymmetry management on a hemisphere-cylinder forebody, *AIAA paper*, 97-1973, 1997.
4. B.L. Smith and A. Glezer, Vectoring and small-scale motions effected in free shear flows using synthetic jet actuators, *AIAA paper*, 97-0213, 1997.
5. A. Tuck, J. Soria, Active flow control of a NACA 0015 airfoil using a ZNMF jet, AIAA Australian Aerospace Student Conference 2004, University of Sydney, 12 December 2004.
6. G. Hong, C. Lee, Q.P. Ha, A.N.F. Mack and S.G Mallinson, Effectiveness of synthetic jets enhanced by instability of Tollmien-Schlichting waves, *AIAA paper*, 2002-2832, 2002.
7. L.D. Kral, Active Flow Control Technology, ASME Fluids Engineering Technical Brief, 2000.
8. A. Seifert, V. Theofilis and R.D. Joslin, Issues in active flow control: theory, simulation and experiment, *AIAA paper*, 2002-3277, 2002.
9. Kral, L.D., Donovan, J.F., Cain, A.B., Cary, A.W., "Numerical simulation of synthetic jet actuator", AIAA paper 97-1824, 28th AIAA Fluid Dynamics Conference, Snowmass Village, CO, June 29 – July 2, 1997.
10. D.A. Lockerby, P.W. Carpenter, Modeling and design of microjet actuation, *AIAA Journal*,

Vol. 42, No. 2, pp220-227, February 2004.

11. R. Mittal, P. Rampunggoon, H.S. Udaykumar, Interaction of a synthetic jet with a flat plate boundary layer, *AIAA paper*, 2001-2773, 2001.
12. D.P. Rizzetta, M.R. Visbal, M.J. Stanek, Numerical investigation of synthetic jet flowfields, *AIAA paper*, 98-2910, 29th AIAA Fluid Dynamics Conference, Albuquerque, NM, June 15-18, 1998.
13. M. Gad-el-Hak, *Flow Control: Passive, Active and Reactive Flow Management* (section 8.10.2), Cambridge University Press, Cambridge, 2000.
14. J.A. Redford, M.W Johnson, Predicting transitional separation bubbles, *Proc. TURBOEXPO 2004*, International Gas Turbine Congress, Austria, 14-17 June 2004.
15. W.P. Wolfe and S.S. Ochs, CFD calculations of S809 aerodynamic characteristics, *AIAA paper*, 97-0973, 1997.
16. B.G. Allan, M. Holt, A. Packard, Simulation of a controlled airfoil with jets, NASA/CR-201750, ICASE Report No. 97-55, October 1977.
17. D.Parekh, S. Palaniswamy, U. Goldberg, Numerical simulation of separation control via synthetic jets, *AIAA paper*, 2002-3167, 2002.
18. A.M. Honohan, M. Amitay, A. Glezer, Aerodynamic control using synthetic jets, *AIAA paper*, 2000-2401, 2000.
19. B.R. Ravi, R. Mittal and F.M. Najjar, Study of three-dimensional synthetic jet flow fields using direct numerical simulation, 42nd AIAA Aerospace Sciences Meeting and Exhibit, Reno, NV, 5-8 January, 2004.
20. U. Rist, On instabilities and transition in laminar separation bubbles, *Proc. CEAS Aerospace Aerodynamics Research Conference*, Cambridge, UK, 10 – 12, June 2002.
21. Y. Na and P. Moin, Direct Numerical Simulation of a Separated Turbulent Boundary Layer, *J. Fluid Mech*, vol. 374, pp. 379-405, 1998.
22. M. Alam and N.D. Sandham, Direct Numerical Simulation of 'Short' Laminar Separation Bubbles with Turbulent Reattachment, *J. Fluid Mech*, vol. 403, pp. 223-250, 2000.
23. J.G. Wissink and W. Rodi, DNS of Transition in a Laminar Separation Bubble, In I. P. Castro and P.E. Hancock, editors, *Advances in Turbulence IX, proceedings of the Ninth European Turbulence Conference*, CIMNE, 2002.
24. A. Hatman and T. Wang, A Prediction Model for Separated-Flow Transition, *ASME paper*, GT-29-237, ASME Turbo Expo '98', Stockholm, Sweden, 1998.
25. M. Gaster, The Structure and Behaviour of Laminar Separation Bubbles, A.R.C. R&M Report No. 3595, 1969.
26. R.J. Shyne, K. Sohn and K.J. Witt, Experimental investigation of boundary layer behaviour in a simulated low pressure turbine, *Journal of Fluids Engineering*, ASME, vol. 122, 84-88, 2000.